ELSEVIER

International Journal of Heat and Fluid Flow 23 (2002) 487–496

International Journal of HEAT AND FLUID FLOW

www.elsevier.com/locate/ijhff

An experimental investigation of buoyancy-opposed wall jet flow

S. He, Z. Xu, J.D. Jackson *

School of Engineering, University of Manchester, Simon Building, Oxford Road, Manchester, M13 9PL, UK

Received 29 June 2001; accepted 13 November 2001

Abstract

An experimental study is reported of the flow and thermal fields produced by injecting a plane jet of warm water down one wall of a vertical passage of rectangular cross section into a slowly moving upward stream of cooler water. Flow visualisation and particle image velocimetry techniques were used to obtain pictures of the flow. This was found to be turbulent and non-steady under certain conditions. Detailed measurements of local mean velocity, turbulence quantities and temperature were made using a laser Doppler anemometry system and a traversable rake of thermocouples. In the regions where the warm water encountered the cooler water the variation of temperature with time was highly intermittent. As Richardson number was increased, the influence of the buoyancy, opposing the flow, had the effect of stabilising it and restricting the downward penetration of the jet and its lateral spread. In the case of the experiments with the higher values of Richardson number a very concentrated shear layer was formed at the interface between the two flow streams. The turbulence was strongly modified in this region, its intensity peaked and the turbulent shear stress changed sign. © 2002 Elsevier Science Inc. All rights reserved.

1. Introduction

The velocity field generated by injecting a buoyancy-opposed plane jet down a vertical wall has some of the characteristics of flows encountered in certain gas-cooled nuclear reactors where hot fluid leaving the core is diverted down the inside surface of a pressure vessel into a space containing slowly moving or even stagnant cooler fluid. With this kind of application in mind, a program of experimental work on buoyancy-influenced wall jet flow was initiated at the University of Manchester with the aim of producing data which could be used for establishing trust in CFD codes which are used in industry to study such flows.

In the investigation reported here, a two-dimensional wall jet flow was produced in a confined space by injecting warm water down one wall of a vertical plane passage into a slowly moving upward stream of cooler water. The instantaneous flow structure was examined using laser light sheet visualisation and particle image velocimetry (PIV). The flow and thermal fields were studied by making detailed measurements of velocity and temperature using a two-component laser Doppler anemometer system and a traversable rake of thermocouples.

Since the pioneering study of Glauert (1956) much research has been done on wall jets. However, the particular aspect of the topic studied in the present investigation, buoyancy-opposed wall jet flow, has received surprisingly little attention. Comprehensive reviews of early work on buoyant vertical jets and wall jet flows were published by Chen and Rodi (1980) and Launder and Rodi (1981), respectively. In the review of Chen and Rodi only one investigation dealing with negative buoyancy was identified (Turner, 1966) and this was limited to flow visualisation. The first study of buoyancy-opposed wall jet flow appears to have been that by Goldman and Jaluria (1986). They made measurements of mean velocity and temperature using hot-wire anemometry and thermocouples, respectively and also reported some flow visualisation studies using smoke. The normalised jet penetration (δ/D) was correlated as a function of Richardson number (Gr/Re^2) and fitted by the following relationship:

$$\frac{\delta}{D} = 4.424\left(\frac{Gr}{Re^2}\right)^{-0.389} \tag{1}$$

* Corresponding author. Tel.: +44-161-275-4307; fax: +44-161-275-4328.

E-mail address: jdjackson@man.ac.uk (J.D. Jackson).

0142-727X/02/$ - see front matter © 2002 Elsevier Science Inc. All rights reserved.
PII: S0142-727X(01)00152-7

Nomenclature

D	jet width
g	gravitational acceleration
Gr	Grashof number
P	shear stress production
Re	Reynolds number
Ri	Richardson number
T	temperature
x	horizontal co-ordinate
y	vertical co-ordinate
$\overline{u}$	horizontal component of RMS turbulent fluctuation velocity
U	horizontal component of local mean velocity
$\rho\overline{u}\overline{v}$	turbulent shear stress
$\overline{v}$	vertical component of RMS turbulent fluctuation velocity
V	vertical component of local mean velocity
$\overline{V}_j$	average velocity at the jet injection location
Greeks	
δ	jet penetration distance
ρ	density
ε	lateral spread of jet
v	kinematic viscosity
Subscripts	
j	jet exit
c	counter-current stream inlet

Goldman and Jaluria found that their data on mean temperature in the jet front mixing layer was very scattered. They attributed this to the unsteadiness of the flow in that region, which was apparent from their flow visualisation studies. A related study was reported by Kapoor and Jaluria (1989). They investigated the heat transfer characteristics of a negatively buoyant two-dimensional wall jet and found that jet penetration and rates of heat transfer both decreased with the increase of buoyancy influence. A more complicated wall jet flow in which, a horizontal wall jet turned downwards at a corner to form a vertical wall jet, was also studied by the same authors (Kapoor and Jaluria, 1991).

More recently, flow visualisation techniques and PIV have been used to examine the flow structures in plane wall jets. Gogineni and Shih (1997) reported such studies in transitional flow regimes. In particular, the interactions between the inner and outer layers of wall jets were investigated. The flow was found to undergo transition from a laminar to a turbulent condition when the Reynolds number based on average velocity and channel width was greater than 2200.

Hsiao and Sheu (1994) investigated the behaviour of double-row vortical structures in the near field region of a plane wall jet. They used flow visualisation and also phase averaging techniques applied to hot-wire measurements. Pictures of the development of vortices along the jet wall and of the ejection of vortices from the wall region were presented by these authors. The results clearly reveal the unsteady nature of such flows.

Balachandar et al. (1992) and Volchkov et al. (1995) studied the flow produced by injecting a wall jet into an approaching stream. The flow configuration considered was similar in some respects to that used in the present study. However no significant buoyancy influences were involved. The effect of the counter-current stream on the jet flow was found to be weak when the ratio of background velocity to jet velocity was less than about 0.1.

2. Experimental facility and instrumentation

Figs. 1 and 2 show the flow circuit, measurement systems and test section used in the present study. The flow circuit consisted of a tank from which two separate streams of water could be pumped to the test section, one through an electrical immersion heater unit having a power rating of up to 108 kW, and the other through a water-cooled shell and tube heat exchanger capable of removing that amount of power. Each stream passed through a flow control valve and an orifice plate flowmeter. The test section, which was a vertical passage of rectangular cross section (breadth 1.2 m, width 0.3 m and height 2.3 m), had transparent walls to enable laser optical measurements of the flow to be made. As shown in Fig. 2, a plane jet of warm water issuing downwards from an 18 mm gap between a glass plate of thickness 20 mm and one wall of the test section encountered a slowly ascending stream of cooler water. Spreading and deceleration of the jet flow occurred until it eventually turned upwards on joining the counter-current stream. The combined flow was withdrawn from the top of the test section. The aspect ratio of the jet was 67:1 and that of the test section was 4:1. It was considered that with such an arrangement the middle region of the flow would be approximately two-dimensional.

An optical arrangement of the kind shown in Fig. 1 was used for visualising the flow field. This utilised a 4 W Argon-ion laser as its light source. The beam was brought to the side of the test section by means of a mirror and lens arrangement, where it encountered a chopper. The beam was then converted into a light sheet of thickness 1.5 mm and width 600 mm, using a cylindrical glass rod. The light sheet passed through the test section mid-way between the temperature and velocity measurement planes ($z = 150$ mm). Two different image recording methods were available. The first utilised a CCD camera connected to an image grabber card on a

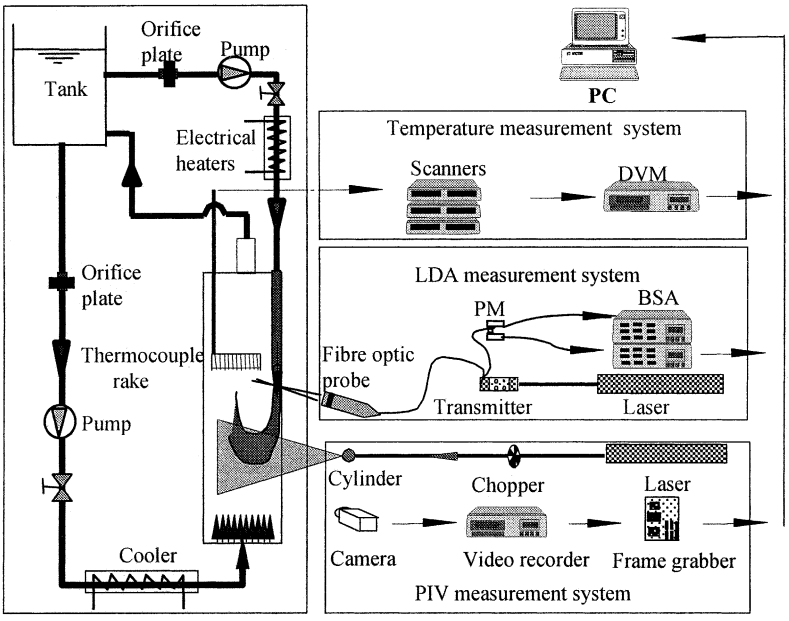

Fig. 1. Flow circuit and measurement systems.

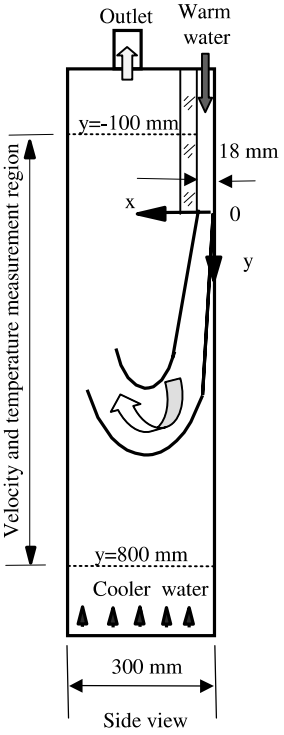

Fig. 2. Side view of test section.

PC. With this arrangement, digital PIV measurements could be made, but only over a limited region of the flow field. The second method utilised a film camera in conjunction with a 35 mm film scanner. This enabled the whole flow field to be visualised.

For laser Doppler anemometry, a two-colour, two-component system of the kind shown in Fig. 1 was used in the back scatter mode. This incorporated a fibre optic probe and two burst spectrum analysers. The probe was mounted on a precision traversing mechanism which enabled the measurement volume to be accurately located at any chosen location within the flow field. The beams were introduced through one side of the test section (i.e., perpendicular to the xy plane) and arranged so that velocities were measured in directions at angles of $\pm 45°$ to the vertical. The vertical and horizontal components of velocity were obtained by making a simple transformation at the data processing stage. The size of the probe volume was $0.122 \times 0.122 \times 8.526$ mm^3, the longest dimension being in the direction, in which the mean flow was uniform, i.e., the z direction.

Considerable attention was devoted to conditioning the flow in the background stream and the jet. At the bottom of the test section a number of graded perforated plates were installed along with a honeycomb flow straightener and multiple layers of mesh to try to produce an approximately uniform background stream. The distributions of the velocity in the x direction were measured using laser Doppler anemometry at various locations in the z direction without any jet flow being injected. The velocity profiles were all found to be slightly inverted (the peak values near each wall being higher than in the centre line value by about 20%). The spatially integrated mean values of the profile did not vary much except for values of z greater than about 550 mm. They are within about 10% of the average value of velocity for the whole flow based on the mass flow rate measurement.

In the case of the jet flow, the intention was to produce a fully developed condition at the injection location

where the jet was injected into the test section. To achieve this, a hydrodynamic development section of length 600 mm (i.e., 33 jet widths) was provided. The flow development section was preceeded by a flow conditioning unit similar to that used at the bottom of the test section for the background stream. The uniformity of the jet flow in the z direction was studied using LDA. The variation was found to be small (less than 5%), outside of the side wall boundary layer region.

The problem of the influence on velocity measurement of non-uniformity of refractive index due to variations of temperature in the water was given careful consideration. A number of measures were taken to minimise such effects. Firstly, the experimental conditions were chosen so as to keep the maximum temperature difference within the water less than 10 °C. Thus, in order to achieve a sufficiently strong buoyancy influences in the experiments, relatively low values of jet flow rate had to be used. Secondly, in order to minimise the laser beam path lengths through the water the measurement plane was chosen to be off-centre from the mid plane of the test section by 350 mm towards the wall where the laser beams were introduced. The location was decided upon in the light of measurements made at the commissioning stage. The plane chosen was within the region where any influence of the side wall was weak, so that the velocity field would be essentially the same as at the mid-plane. By this means, the path of the laser beams through the water was limited to 250 mm. Finally, the sampling of data from the two individual channels of the LDA system was synchronised. Signals were only considered to be valid when received at the same time from both of the burst spectrum analysers. By doing this, the likelyhood of measuring the velocity at locations other than the one prescribed was small and false fluctuations of velocity due to fluctuations of the refractive index were largely eliminated. The use of burst spectrum analysers in this study proved to be extremely beneficial. Ramaprian and Chandrasekhara (1985) reported difficulties in making reliable LDA measurements using a tracker system to study flow fields in water with significant temperature gradients. They had to develop an arrangement involving glass tubes within the water to take the laser beams through most of the path.

A consequence of the approach used in making the LDA measurements was that the sampling frequency was very low, especially in the experiments with the larger temperature differences (only a few Hertz in the worst cases). In the early stages of the experimental program, a range of sampling time periods were tried. It was found that 5 min gave satisfactorily converged measurements for most of the cases tested. Therefore, this value was chosen for use throughout the remaining experimental program. In order to represent the sampling time in a normalised form, a macro time scale based on the mean flow can be used. Choosing channel width and the jet velocity as the length and velocity scales, the normalised value is of the order of 100 for a sampling time of 5 min.

Thermocouples were used for mapping the temperature field. The distribution of temperature along the jet wall was measured using eleven fixed thermocouples with the hot junctions situated in the water quite near to the test section surface. The distribution of temperature over the whole flow field was measured in the mid plane of the test section ($z = 0$) using a motor driven traversable rake carrying twenty one 'fast response' thermocouple junctions, made of wire of diameter only 0.076 mm. As shown in Fig. 1, the thermocouple signals were supplied to a 60 channel, computer-based scanning system connected to a precision, microprocessor controlled digital voltmeter.

3. Experimental investigation

It can be shown that for a buoyancy-influenced flow of the kind under consideration here two-dimensionless groups appear in the governing equations when they are represented in non-dimensional form. These are Reynolds number and Grashof number, which are defined, here respectively, as:

$$Re = \frac{\overline{V}_j D}{\nu_j}, \tag{2}$$

in which $\overline{V}_j$ is the average velocity of the jet flow at the injection location, and

$$Gr = \frac{gD^3(\rho_c - \rho_j)/\rho_j}{\nu_j^2}. \tag{3}$$

For buoyant jet flows the Richardson number Ri $(= Gr/Re^2)$, which can be thought of in terms of the ratio of buoyancy force to inertia force, is sometimes used in the place of Grashof number. Expressed in terms of the basic variables this is

$$Ri = \frac{gD(\rho_c - \rho_j)/\rho_j}{\overline{V}_j^2}. \tag{4}$$

Another parameter needed to characterise the flow under consideration here is the ratio of background velocity to jet velocity $V_c/\overline{V}_j$. In the present study this was kept constant at a sufficiently small value of about 0.077 to ensure that the counter-current flow would only have a weak influence on the overall flow field.

Reynolds number and Grashof number were both varied systematically in the experiments reported here. This was done by controlling the velocities of the jet flow, the background flow and the jet to background fluid temperature difference. The velocity of the jet flow was varied from about 0.10–0.21 m/s and the difference of temperature between the jet flow and the counter-

Table 1
Experimental conditions

Test	*Re*	*Gr*	*Ri*	V_j (m/s)	V_c (m/s)	T_j (°C)	T_c (°C)
1	4754	0	0	0.167	0.013	42	42
2	4754	234000	0.01	0.167	0.013	42	38
3	6000	468000	0.013	0.210	0.016	42	34
4	4754	468000	0.02	0.167	0.013	42	34
5	3000	234000	0.026	0.105	0.008	42	38
6	4000	468000	0.029	0.140	0.011	42	34
7	3000	468000	0.052	0.105	0.008	42	34

Note: the quoted velocity values in the above table are averaged ones based on measured mass flow rates of jet and background flows.

current flow was varied from 4° to 10°. The fluid temperature at the jet injection location was kept constant at 42 °C in all the experiments by adjusting the flow rate of the cooling water supplied to the shell and tube heat exchanger. As a result, the Reynolds number of the jet flow varied in the range 3000–6000 and Grashof number varied in the range 234 000–468 000. Thus, Richardson numbers in the range 0.01–0.052 were achieved. The experimental conditions covered in the experiments reported here are summarised in Table 1.

4. Results and discussion

4.1. Flow structure

In the first place, the PIV system was used in flow visualisation experiments to study the instantaneous flow structure. Experiments were conducted under both isothermal and non-isothermal conditions. It was found that for isothermal conditions, and also for non-isothermal conditions with small temperature difference, the flow pattern was clearly not steady. Large vortices, which sometimes penetrated deep into the flow field, were seen to be randomly superimposed on the main flow pattern. As the jet to background stream temperature difference was increased, influences on the flow of buoyancy became evident. Jet penetration and lateral spread were both systematically reduced. The flow pattern was then steadier and more clearly apparent. Superimposed vortices were seen less frequently. Under such conditions, the warm jet fluid was inhibited by buoyancy from interacting freely with the cooler fluid in the background flow.

4.2. The mean flow field

Fig. 3(a)–(c) show mean flow velocity vector fields for an isothermal condition ($Ri = 0$) and two non-isothermal conditions ($Ri = 0.01$ and 0.02) which span a range of buoyancy influence from weak to moderately strong. In each case the flow pattern is clearly apparent. After being injected downwards on the right-hand wall near the top of the test section (location $y = 0$), the jet flow spreads and decelerates. It eventually turns upwards and combines with the counter-current stream. The combined flow leaves the test section at the top in the central region. For the isothermal case ($Ri = 0$, Fig. 3(a)), it can be seen that the jet flow penetrates right down to the bottom of the test section. However, with increase of Richardson number both the penetration of the jet and its lateral spread are systematically reduced.

Fig. 4 shows profiles at various heights in the test section of the vertical component of local mean velocity, normalised using the average velocity of the jet flow. The flow field can be conveniently considered in three parts, a wall jet flow region, a mixing region between the wall jet flow and the counter-current stream and a return flow region. These can each be clearly identified. In the wall jet region on the right, the velocity is downwards and is relatively large but decays with reduction of height. With the increase of Richardson number, this decay occurs more quickly and the penetration of the jet is reduced. The velocity falls to zero in the mixing region beyond the edge of the jet front.

The velocity profile in the return flow region also changes with increase of Richardson number. For isothermal conditions ($Ri = 0$, Fig. 4(a)), the maximum upward velocity occurs at a location close to the far wall. The velocity then decreases slowly with distance from that wall. With the increase of Richardson number, the location of the maximum velocity in the return flow shifts away from the far wall. The acceleration of the fluid in the middle of the test section occurs as a result of the influence of buoyancy, which is significant in that region.

Fig. 5 shows the variation with height of normalised downward velocity at a distance 14 mm from the jet wall for various values of Richardson number. Three stages can be identified. Below the jet exit there is a development region in which the velocity decays relatively slowly. Further down, at a distance which depends on Richardson number, the decay of velocity becomes much greater due to mixing. Eventually the velocity becomes negative, indicating that the region of the counter-current flow has been reached. It is clear that the greater the buoyancy influence, the earlier the velocity variation changes from the first to the second stage. It can also be seen that

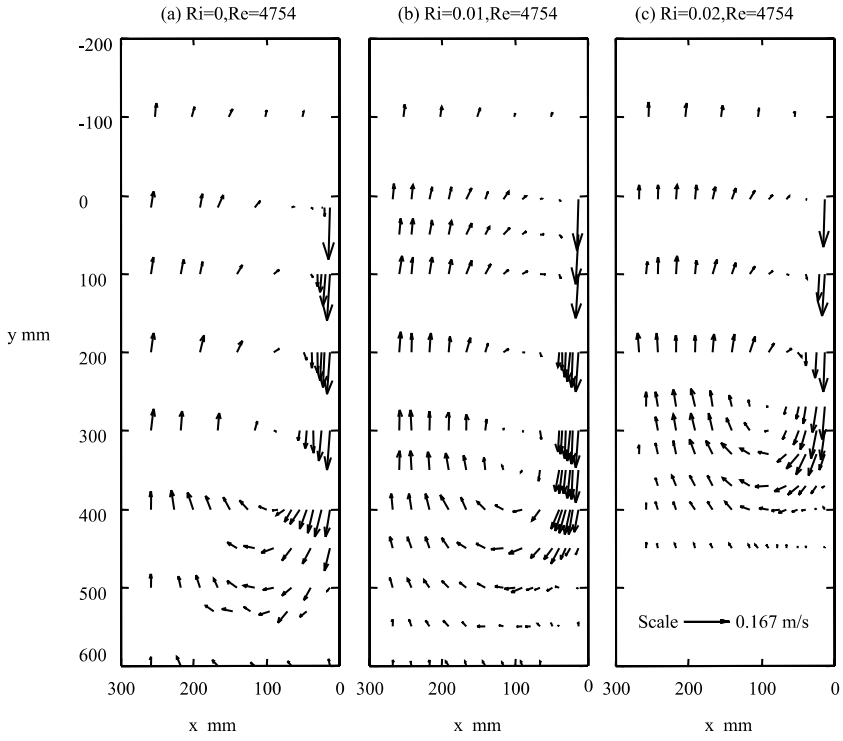

Fig. 3. Mean velocity vector field.

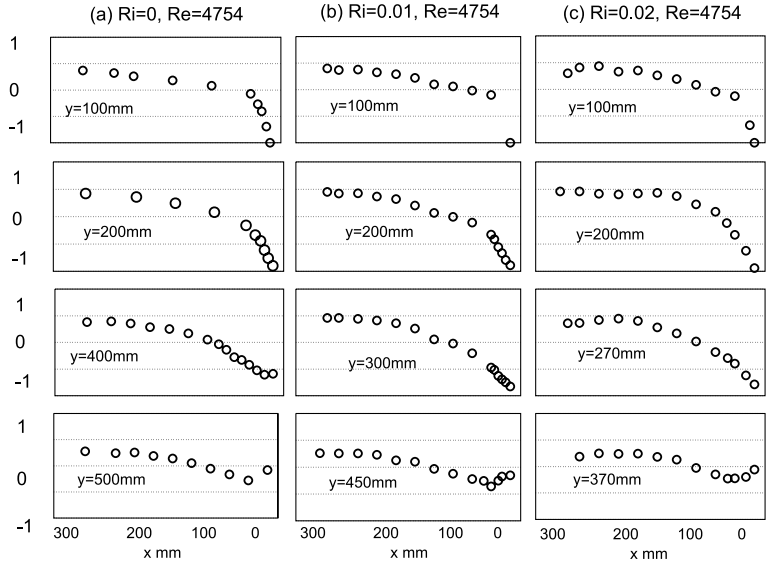

Fig. 4. Profiles of normalised values of vertical component of local mean velocity.

the higher the Richardson number, the steeper is the velocity variation within the mixing region. For the case of the highest value of Richardson number, the velocity starts to fall quickly almost immediately below the jet injection location. The flow immediately turns and bends away from the wall. In this case, there is virtually no jet development region. It is interesting to note that, for the cases where $Ri \leqslant 0.026$, the values of velocity within the wall jet development region collapse onto the same curve indicating that the flow in that region is not significantly affected by buoyancy.

4.3. The turbulence field

Fig. 6 shows the root-mean-square values of the vertical and horizontal components of turbulent velocity

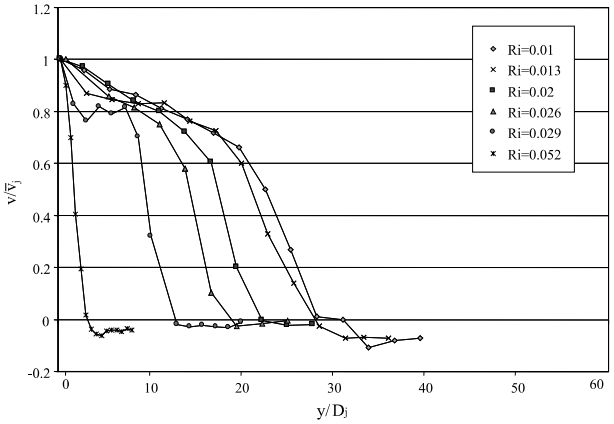

Fig. 5. Decay of normalized velocity in the jet flow.

fluctuation normalised using the average velocity of the jet at the injection location. The distributions of turbulence intensity are generally fairly uniform above the mixing region. Even in the re-circulation zone, where the mean velocity is low, the normalised RMS velocities remain at a level similar to those in the other regions. It is interesting to note that the RMS velocity is enhanced in the jet frontal area, particularly for strongly buoyancy-influenced case.

The turbulent shear stress (not shown here) generally shows features consistent with those found in the case of the normal stresses. In particular, high levels of turbulent shear stress are generated in both the wall jet and the mixing regions in all test cases, although the locations of these regions of high stress shift as a result of buoyancy influences.

Buoyancy has a clear impact on the shear stress in the return flow region. For the isothermal case, and also for case with weak buoyancy influence, the turbulent shear stress in this region is relatively small. It approaches zero at the measurement location nearest to the wall and increases only slightly with distance from the wall. For the cases with strong buoyancy influence significant negative turbulent shear stress is generated in the region near the far wall. This can be related to the mean flow field. As noted earlier, the maximum upward velocity in the return flow region shifts away from the far wall with the increase of Richardson number (see Fig. 4). Consequently, in the region approaching that wall, the gradient of mean velocity changes sign with increase of buoyancy influence. The shear stress changes sign as well.

4.4. The temperature field

Distributions of normalised values of local mean temperature down the jet wall are shown in Fig. 7 for the full range values of Richardson number covered in the experiments. These are generally similar to the distributions of velocity in the jet flow shown earlier in Fig. 5. The temperature decays slowly at first but then falls within a relatively short distance to that of the counter-current flow. The greater the Richardson number, the shorter is the distance that the wall remains at the higher temperature and the more sharply the temperature then falls. It can be seen that the temperature distribution above the region where the sharp fall of temperature occurs is similar for each of the cases shown in Fig. 7. This adds weight to the suggestion made earlier that the

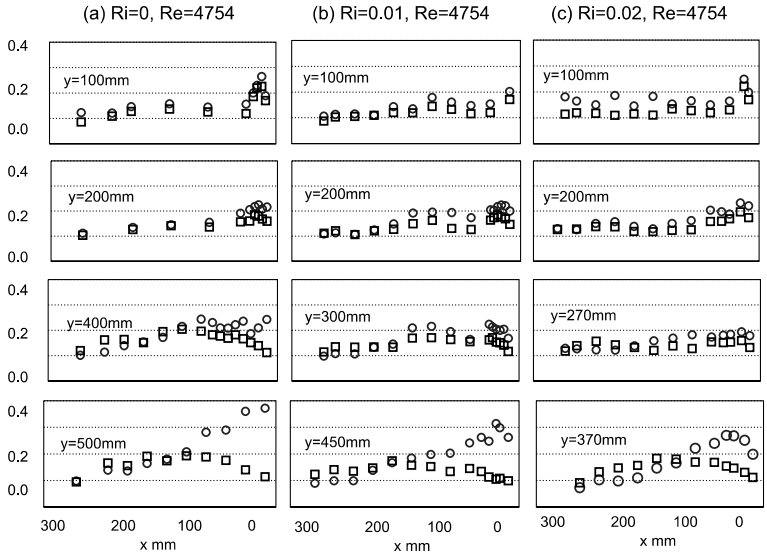

Fig. 6. Profiles of normalised vertical and horizontal components of local RMS velocity fluctuation (○: vertical component, □: horizontal component).

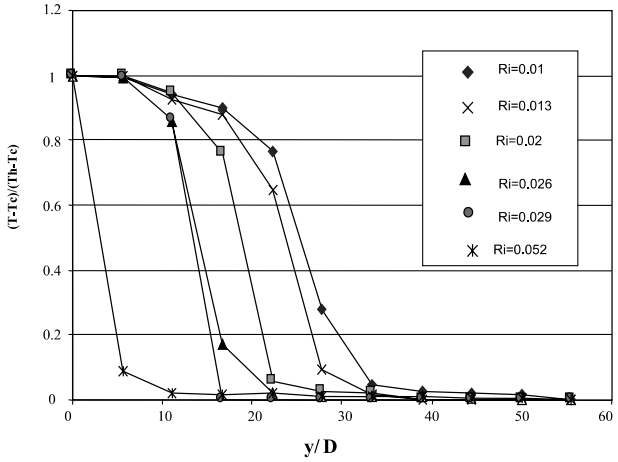

Fig. 7. Decay of normalised wall temperature.

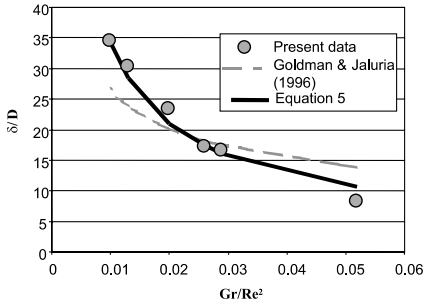

Fig. 8. Penetration of jet.

initial development of the jet is not affected much by buoyancy. In fact, the temperature contours obtained (not presented here) show that although, the warm jet fluid is restricted to a smaller region with increase of buoyancy influence there is little variation of temperature across the jet flow even for the case with the higher Richardson number. Consequently, there is little direct buoyancy influence on the flow within the jet.

Fig. 8 shows the variation with Richardson number of normalised jet penetration determined from measurements of the temperature field. The penetration of the jet is defined rather arbitrarily as the distance from the jet exit to the location at which the normalised value of wall temperature minus background stream temperature falls to about a value of 0.02. The following relationship was found to fit our data satisfactorily,

$$\frac{\delta}{D} = 1.288\left(\frac{Gr}{Re^2}\right)^{-0.713}. \quad (5)$$

Also shown on Fig. 8 is the curve given by, the equation of Goldman and Jaluria (1986). Clearly, the reduction of jet penetration with the increase of the Richardson number found in the present study is stronger than that found by Goldman and Jaluria. This is not surprising

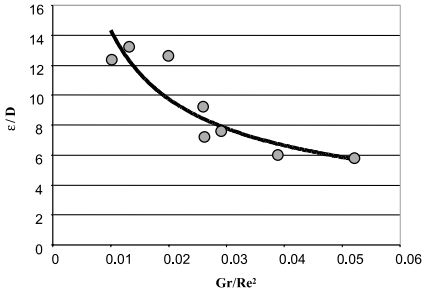

Fig. 9. Lateral spread of jet.

when one considers the differences between the arrangements used in the two experiments. That of Goldman and Jaluria was open both at the top and bottom. The rate at which fluid was drawn from the bottom of the test section was dependent on the experimental conditions, whereas in the present experiment it was controlled. Although this is probably the main difference between the two experiments which would have had a significant effect, other differences such as the aspect ratio of the test section could have contributed as well.

The influence of buoyancy on the lateral spread of the jet is shown in Fig. 9. To determine this, the distance from the jet wall to the location where the maximum vertical component of velocity occurred was first determined for various heights. In general this distance varied with height. The maximum value was used to define the jet lateral spread. As can be seen, the scatter of the points on Fig. 9 is relatively large. This is due to the fact that, in some cases, the velocity profile was very flat and therefore it was difficult to decide accurately on the location at which the maximum velocity was achieved. Nevertheless, it is clear from the results that the lateral spread of the jet does reduce in a systematic manner with increase of Richardson number.

The variation with time of local fluid temperature at the height $y = 220$ mm and various horizontal positions is shown in Fig. 10 for a condition of relatively strong buoyancy influence, $Gr/Re^2 = 0.026$. It can be seen that, in the mixing region, the fluid temperature switches intermittently between two values, one close to that of the jet and one close to that of the counter-current stream. The local time mean temperatures referred to earlier in the discussion of Fig. 7 are merely nominal in the mixing region. In reality, the fluid does not actually take up steady values of temperature in the regions where warm fluid encounters cooler fluid.

Fig. 11 shows histograms of the variation of the fluid temperature at various heights and various horizontal positions. The intermittency of the temperature variations in the mixing region shows up as double peaks in this form of presentation. Outside the mixing region, the histograms show only a single peak concentrated at either the jet or the background fluid temperature.

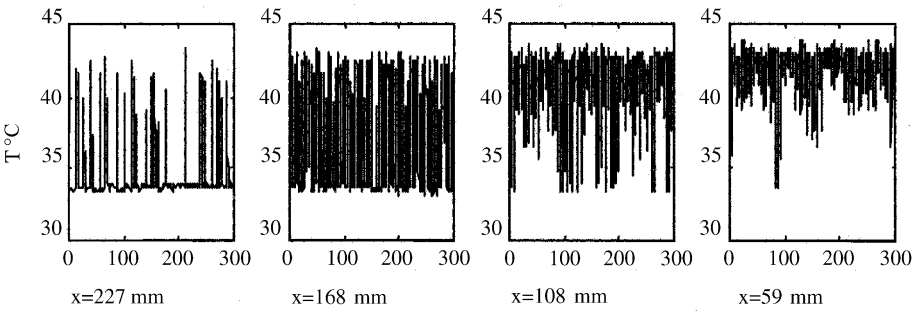

Fig. 10. Temperature variation with time at $y = 200$ mm ($Ri = 0.026$, $Re = 4754$, $V_c/V_j = 0.07$).

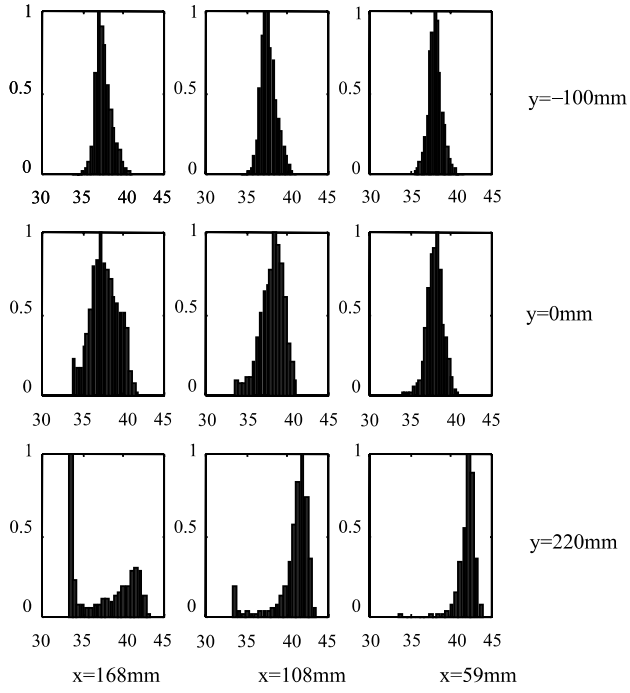

Fig. 11. Histograms of temperature at various locations ($Ri = 0.026$, $Re = 4754$, $V_c/V_j = 0.07$).

5. Conclusions

Detailed measurements of local mean velocity, turbulence and temperature have been successfully made using laser Doppler anemometry and thermocouples, respectively, in the flow field produced by a buoyancy-opposed wall jet discharging into a slowly moving counter-current stream in a vertical test section of plane geometry.

Laser optical flow visualisation techniques have enabled pictures to be obtained of the instantaneous flow field. This was found to be very turbulent and rather unsteady under conditions of zero or small buoyancy influence.

Buoyancy had the effect of stabilising the flow and reducing the extent of the mixing region. Jet penetration and lateral spread were both systematically reduced as a result of increasing the buoyancy influence.

When the buoyancy influence was very strong, a very concentrated mixing layer was formed at the interface between the two flow streams. The turbulence field was strongly modified in this region, the intensity of turbulence peaked and turbulent shear stress changed sign.

The temperature varied with time in a highly intermittent manner in the regions where warm fluid from the jet encountered cooler fluid from the counter-current stream.

Acknowledgements

The work reported here was supported by a research contract entitled 'Generic Studies of Thermal Convention—CFD Quality and Trust' funded jointly by British Energy Generation Ltd. and BNFL Magnox Generation on behalf of the UK Nuclear Industry Management Committee (IMC). The authors gratefully acknowledge the support received.

References

Balachandar, R., Robillard, L., Ramamurthy, A.S., 1992. Some characteristics of counter flowing wall jets. ASME J. Fluids Engng. 114, 554–558.

Chen, C.J., Rodi, W., 1980. Vertical Turbulent Buoyant Jets: A Review of Experimental Data. Pergamon Press, New York.

Glauert, M.B., 1956. The wall jet. J. Fluid Mech. 1, 625–643.

Gogineni, S., Shih, C., 1997. Experimental investigation of the unsteady structure of a transitional plane wall jet. Exp. Fluids 23, 121–129.

Goldman, D., Jaluria, Y., 1986. Effect of opposing buoyancy on the flow in free and wall jets. J. Fluid Mech. 166, 41–56.

Hsiao, F.B., Sheu, F.B., 1994. Double row structures in the near field region of a plane wall jet. Exp. Fluids 17, 291–301.

Kapoor, K., Jaluria, Y., 1989. Heat transfer from a negatively buoyant wall jet. Int. J. Heat Mass Transfer 32, 697–709.

Kapoor, K., Jaluria, Y., 1991. Mixed convection flow due to a buoyant wall jet turning downward at a corner. In: Mixed Convection Heat Transfer, HTD, vol. 163. ASME, New York, pp. 119–128.

Launder, B.E., Rodi, W., 1981. The turbulent wall jet. Prog. Aerospace Sci. 19, 81–128.

Ramaprian, B.R., Chandrasekhara, M.S., 1985. LDA measurements in plane turbulent jets. ASME J. Fluids Engng. 107, 264–271.

Turner, J.S., 1966. Jets and plumes with negative or reversing buoyancy. J. Fluid Mech. 26 (part 4), 770–792.

Volchkov, E.P., Lebedev, V.P., Nizovtsev, M.I., Terekhov, V.I., 1995. Heat transfer in a channel with a counter-current wall jet injection. Int. J. Heat Mass Transfer 38, 2677–2687.